Dinuclear lanthanoid(III) dithiocarbamato complexes bridged by (*E*)-*N*-benzylidenepicolinohydrazonate: syntheses, crystal structures and spectroscopic properties

Abdallah Yakubu,[a] Takayoshi Suzuki,[a,b,*] Masakazu Kita[c]

[a] Graduate School of Natural Science and Technology, Okayama University, 3-1-1 Tsushima-Naka, Kita-ku, Okayama 700-8530, Japan

[b] Research Institute for Interdisciplinary Science, Okayama University, 3-1-1 Tsushima-Naka, Kita-ku, Okayama 700-8530, Japan

[c] Faculty of Education, Okayama University, 3-1-1 Tsushima-Naka, Kita-ku, Okayama 700-8530, Japan

Abstract

(*E*)-*N*-Benzylidenepicolinohydrazide (Hbphz) was used to synthesize a series of hydrazonato-bridged homodinuclear Ln^{III}_2 dithiocarbamato (*RR*′dtc$^-$) complexes of the form [{Ln(*RR*′dtc)$_2$}$_2$(μ-bphz)$_2$] {Ln = La, Pr, Nd, Sm or Eu; *RR*′ = dimethyl- (Me_2) or pyrrolidine- (pyr)}. X-ray crystallographic studies revealed that these complexes possessed a common head-to-tail type dinuclear structural motif in which two hydrazonato ligands bridged two Ln^{III} centers in the μ-1κ^2*N*(py),*O*:2κ^2*O*,*N*(imine) mode and two *RR*′dtc ligands coordinated to each Ln^{III} center. Interestingly, while the Sm^{III} and Eu^{III} complexes crystallized as simple 8:8-coordinate dinuclear molecules, the lighter Ln^{III} (i.e. La^{III}, Pr^{III} and Nd^{III}) complexes afforded in some cases 9:9-coordinate molecules, where the ninth coordination site was occupied by a solvent ethanol or methanol molecule. Even for the lighter Ln^{III} complexes, the complexes were solved in dichloromethane or chloroform as the 8:8-coordinate dimer, as revealed by ^{1}H NMR spectroscopy. In the UV-visible absorption and magnetic circular dichroism (MCD) spectra of the complexes, similar spectral patterns for ligand-centered and Laporte forbidden f–f transitions were observed. The MCD spectral studies demonstrated the characteristic magneto-optical behavior of the complexes.

Keywords: Hydrazone, dithiocarbamate, crystal structures, lanthanoid, magnetic circular dichroism.

1. Introduction

The coordination chemistry of hydrazones is an active research area in view of their general interests and application of hydrazone complexes **[**1,2**]**. Hydrazones can coordinate to a metal center either as neutral molecules or deprotonated anionic forms; therefore, the hydrazone complexes often exhibit interesting reversible properties dependent on the solvent acidity [3,4]. In addition, the exploitation of possible ligating substitutional groups affords a variety of coordination modes of the hydrazones which would give the complexes with interesting structural diversity, magnetic and spectroscopic properties [5].

Lanthanoid complexes of hydrazones are being investigated for potential applications in various fields including supramolecular assemblies and magnetic materials. Chandrasekhar et al. have prepared a series of hydrazone-based homodinuclear lanthanoid complexes and revealed the presence of weak antiferromagnetic coupling between the Ln^{III} centers at low temperature [6]. Thompson and co-authors have investigated the coordination chemistry of tritopic pyridinebis(hydrazone) with some Ln^{III} ions [**7**]. Klouras, Perlepes and their collaborators characterized dinuclear 2-acetylpyridine-substituted hydrazone complexes with four bridging acetate groups [8]. The structural characterizations and magnetic properties of other hydrazone-based dinuclear Dy^{III}_2 [9] and tetranuclear Ln^{III}_4 [10] complexes have also been reported. In addition, several mixed-ligand lanthanoid complexes bearing hydrazones (or the deprotonated hydrazonates) and β-diketonates (or other oxygen-donor ligands) have been reported; however, those of the analogous mixed-ligand complexes with dithiocarbamates have not yet been investigated. Lanthanoid dithiocarbamato compounds have important practical applications in catalysis, nanotechnology and microelectronics, and, therefore, their structural, thermodynamical and spectroscopic properties have been studied in detail [11, 12]. So far, most of the mixed-ligand dithiocarbamato lanthanoid complexes studied involve 1,10-phenanthroline or 2,2'-bipyridine as an ancillary ligand.

In this study, a hydrazone derived from picolinohydrazide and benzaldehyde, (*E*)-*N*-benzylidenepicolinohydrazide (Hbphz) was synthesized and used to prepare a series of lanthanoid dithiocarbamato complexes (Scheme 1). The structural features and spectroscopic properties of these hydrazonato-bridged homodinuclear lanthanoid dithiocarbamato complexes were investigated.

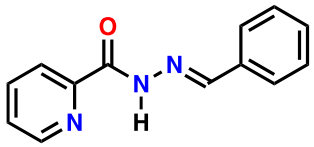

Scheme 1 (*E*)-*N*-benzylidenepicolinohydrazide (Hbphz)

2. Experimental section

2.1 Synthesis of (*E*)-*N*-benzylidenepicolinohydrazide (Hbphz)

2-Pyridinecarboxylic acid hydrazide (= picolinohydrazide) (343 mg, 2.5 mmol) was dissolved in ethanol (20 mL) and benzaldehyde (265 mg, 2.5 mmol) was added. The mixture was stirred for 3 h at room temperature and, then, allowed to stand overnight. A slight shaking of the mixture triggered precipitation of the product. Analytically pure white fluffy product was isolated in 73% yield. Slow evaporation of a methanolic solution of the product yielded colorless needle-shaped crystals suitable for X-ray diffraction analysis. Anal. Found: C, 69.23; H, 4.67; N, 18.55%. Calcd. for $C_{13}H_{11}N_3O$: C, 69.32; H, 4.92; N, 18.66%. IR (KBr disc)/cm^{-1}: ν(N–H), 3212; ν(C=O), 1664; ν(C=N), 1522; ν(N–N), 1141. ^{1}H NMR (300 MHz, Chloroform-*d*, 22 °C): δ 10.99 (s, 1H), 8.58 (ddd, *J* = 4.8, 1.8, 0.9 Hz, 1H), 8.42–8.16 (m, 2H), 8.02–7.64 (m, 3H), 7.60–7.31 (m, 4H).

2.2 Synthesis of complexes

All complexes reported in this article were similarly prepared by a method described below. To a mixture of Hbphz (1.00 mmol) and Et_3N (1.00 mmol) in MeOH (10 mL) was added a methanolic solution (10 mL) of LnX_3•$6H_2O$ (Ln = La, Pr, Nd, Sm or Eu; X^- = Cl^- or NO_3^-) (1.00 mmol) with stirring. Na(Me_2dtc) or NH_4(pyrdtc) (2.00 mmol) in MeOH (10 mL) was added. The mixture was stirred for 5 h at room temperature and the resulting precipitate was

collected by filtration, washed with MeOH and dried in air. The crude product was purified by recrystallization from a dichloromethane or chloroform solution by layering of ethanol, methanol or diethyl ether. The analytical and FT-IR spectral data are given below.

2.2.1 [{La(Me$_2$dtc)$_2$}$_2$(μ-bphz)$_2$] (1a)

Pale green crystals were obtained from a mixture of CH_2Cl_2 and EtOH in 18% yield. Anal. Found: C, 36.29; H, 3.77; N, 11.21; S, 19.30%. Calcd. for $C_{38}H_{44}N_{10}O_2La_2S_8$•$2CH_3OH$•$2H_2O$: C, 36.75; H, 4.32; N, 10.71; S, 19.62%. IR (KBr disc)/cm^{-1}: ν(C=N),1540; ν(N–N), 1161; ν(C–N), 1349; ν(C–S) 982.

2.2.2 [{La(pyrdtc)$_2$}$_2$(μ-bphz)$_2$] (1b)

Pale green crystals were obtained from a mixture of $CHCl_3$ and EtOH in 21% yield. Anal. Found: C, 40.55; H, 3.99; N, 10.37; S, 18.65%. Calcd for $C_{46}H_{52}N_{10}O_2La_2S_8$•$CH_3OH$•$2H_2O$: C, 40.92; H, 4.38; N, 10.15; S, 18.60%. IR (KBr disc)/cm^{-1}: ν(C=N), 1539; ν(N–N), 1163; ν(C–N), 1430; ν(C–S) 1005.

2.2.3 [{Pr(Me$_2$dtc)$_2$}$_2$(μ-bphz)$_2$] (2a)

Green crystals were obtained from a mixture of CH_2Cl_2 and EtOH in 19% yield. Anal. Found: C, 37.23; H, 3.50; N, 11.41; S, 19.85%. Calcd. for $C_{38}H_{44}N_{10}O_2Pr_2S_8$•$0.5CH_2Cl_2$: C, 36.89; H, 3.62; N, 11.17; S, 20.46%. IR (KBr disc)/cm^{-1}: ν(C=N), 1540; ν(N–N), 1158; ν(C–N), 1347; ν(C–S) 979.

2.2.4 [{Pr(pyrdtc)$_2$}$_2$(μ-bphz)$_2$] (2b)

Green crystals were obtained from CH_2Cl_2 and EtOH in 21% yield. Anal. Found: C, 41.49; H, 4.25; N, 9.86; S, 18.90%. Calcd. for $C_{46}H_{52}N_{10}O_2Pr_2S_8$•$2H_2O$: C, 40.88; H, 4.18; N, 10.37; S, 18.98%. IR (KBr disc)/cm^{-1}: ν(C=N), 1540; ν(N–N), 1163; ν(C–N), 1430; ν(C–S) 1006.

2.2.5 [{Nd(Me$_2$dtc)$_2$}$_2$(μ-bphz)$_2$] (3a)

Pale green crystals were obtained from $CHCl_3$ and MeOH mixture in 42% yield. Anal. Found: C, 36.82; H, 3.70; N, 11.16; S, 18.87%. Calcd. for $C_{38}H_{44}N_{10}O_2Nd_2S_8$•$2CH_3OH$•$0.5CHCl_3$: C, 36.26; H, 3.95; N, 10.44; S, 19.12%. IR (KBr disc)/cm^{-1}: ν(C=N), 1543; ν(N–N), 1159; ν(C–N), 1349; ν(C–S) 980.

2.2.6 [{Nd(pyrdtc)$_2$}$_2$(μ-bphz)$_2$] (3b)

Pale green crystals were obtained from CH_2Cl_2 and EtOH mixture in 43% yield. Anal. Found: C, 41.56; H, 4.56; N, 9.78; S, 17.57%. Calcd. for $C_{46}H_{52}N_{10}O_2Nd_2S_8$•$2CH_3CH_2OH$•$CH_2Cl_2$•$H_2O$: C, 41.25; H, 4.62; N, 9.43; S, 17.27%. IR (KBr disc)/cm^{-1}: ν(C=N), 1541; ν(N–N), 1163; ν(C–N), 1431; ν(C–S) 1007. ^{1}H NMR (300 MHz, Chloroform-*d*, 22°C) δ 9.56 (dd, *J* = 14.6, 7.2 Hz, 1H), 8.94–8.23 (m, 2H), 7.99–7.70 (m, 1H), 7.69–7.37 (m, 1H), 7.26 (s, 1H), 4.39–3.40 (m, 8H), 1.67–1.04 (m, 8H).

2.2.7 [{Nd(pyrdtc)$_2$}$_2$(μ-bphz)$_2$] (3b')

Pale green crystals were obtained from CH_2Cl_2 and Et_2O. Anal. Found: C, 41.58; H, 4.00; N, 10.56; S, 19.20%. Calcd. for $C_{46}H_{52}N_{10}O_2Nd_2S_8$: C, 41.79; H, 3.96; N, 10.60; S, 19.40%. IR (KBr disc)/cm^{-1}: ν(C=N), 1544; ν(N–N), 1163; ν(C–N), 1436; ν(C–S) 1004. ^{1}H NMR (300 MHz, Chloroform-*d*, 22°C) δ 9.56 (t, *J* = 10.2 Hz, 1H), 8.89–8.21 (m, 2H), 7.77 (t, *J* = 8.7 Hz, 1H), 7.69–7.37 (m, 1H), 7.26 (s, 2H), 4.27–3.47 (m, 6H), 1.61–1.03 (m, 6H).

2.2.8 [{Sm(Me$_2$dtc)$_2$}$_2$(μ-bphz)$_2$] (4a)

Pale yellow crystals were obtained from $CHCl_3$ and EtOH in 18% yield. Anal. Found: C, 35.97; H, 3.33; N, 10.93; S, 20.37%. Calcd. for $C_{38}H_{44}N_{10}O_2Sm_2S_8$•$0.5CHCl_3$: C, 35.85; H, 3.48; N, 10.86; S 19.89%. IR (KBr disc)/cm^{-1}: ν(C=N), 1545; ν(N–N), 1129; ν(C–N), 1351; ν(C–S) 982.

2.2.9 [{Sm(pyrdtc)$_2$}$_2$(μ-bphz)$_2$] (4b)

Pale yellow crystals were obtained from CH_2Cl_2 and EtOH in 22% yield. Anal. Found: C, 40.69; H, 3.71; N, 10.36; S, 19.06%. Calcd. for $C_{46}H_{52}N_{10}O_2Sm_2S_8$•$0.5CH_2Cl_2$: C, 40.57; H, 3.88; N, 10.17; S, 18.63. IR (KBr disc)/cm^{-1}: ν(C=N), 1545; ν(N–N), 1164; ν(C–N), 1437; ν(C–S) 1005.

2.2.10 [{Eu(Me$_2$dtc)$_2$}$_2$(μ-bphz)$_2$] (5a)

Orange crystals were obtained from $CHCl_3$ and MeOH in 37% yield. Anal. Found: C, 35.12; H, 3.41; N, 10.55; S, 19.20%. Calcd. for $C_{38}H_{44}N_{10}O_2Eu_2S_8$•$CHCl_3$: C, 35.04; H, 3.39; N, 10.48; S, 19.19%. IR (KBr disc)/cm^{-1}: ν(C=N), 1545; ν(N–N), 1131; ν(C–N), 1351; ν(C–S) 982.

2.2.11 [{Eu(pyrdtc)$_2$}$_2$(μ-bphz)$_2$] (5b)

Orange crystals were obtained from $CHCl_3$ and EtOH in 40% yield. Anal. Found: C, 38.03; H, 3.70; N, 9.41; S, 17.23%. Calcd. for $C_{46}H_{52}N_{10}O_2Eu_2S_8$•$CHCl_3$: C, 38.76; H, 3.67; N, 9.62; S, 17.61%. IR (KBr disc)/cm^{-1}: ν(C=N), 1545; ν(N–N), 1165; ν(C–N), 1436; ν(C–S) 1005.

2.3 Physical Measurements

C, H, N and S analysis were carried out on a Perkin Elmer Series II CHNS/O Analyzer 2400 at Department of Instrumental Analyses, Advanced Science Research Center, Okayama University. The FT-IR spectra were recorded on a JASCO FT-001 FT-IR spectrophotometer by a KBr disc method in the 400–4000 cm^{-1} range. The UV-visible absorption spectra of the complexes in dichloromethane were obtained on a JASCO V-550 UV/VIS spectrophotometer at room temperature. Room temperature magnetic circular dichroism (MCD) spectra were measured on a JASCO J-1500 CD spectropolarimeter equipped with a home-made neodymium magnet apparatus (ca. 0.5 T magnetic field) [13].

2.4 X-ray crystallographic study

X-ray diffraction intensity data were collected on a Rigaku R-AXIS Rapid diffractometer, except for those of compound **5b** which were obtained on a Rigaku VariMax diffractometer with a Saturn-70 CCD detector, using graphite or multi-layered mirror monochromated Mo Kα (λ = 0.71075 Å) radiation. The diffraction data were processed using the PROCESS-AUTO or CrystalClear software package [14] and the numerical absorption corrections were applied [15]. The structures were solved by the direct method employing the SIR2008 [16] or SHELXT [17] software package and expanded using Fourier techniques, and refined on F^2 (with all independent reflections) using SHELXL Version 2014/7 software package [18]. All non-hydrogen atoms were refined anisotropically. Hydrogen atoms were introduced at the theoretical positions and refined using riding models. All calculations were performed using the CrystalStructure software package [19].

3. Results and discussion

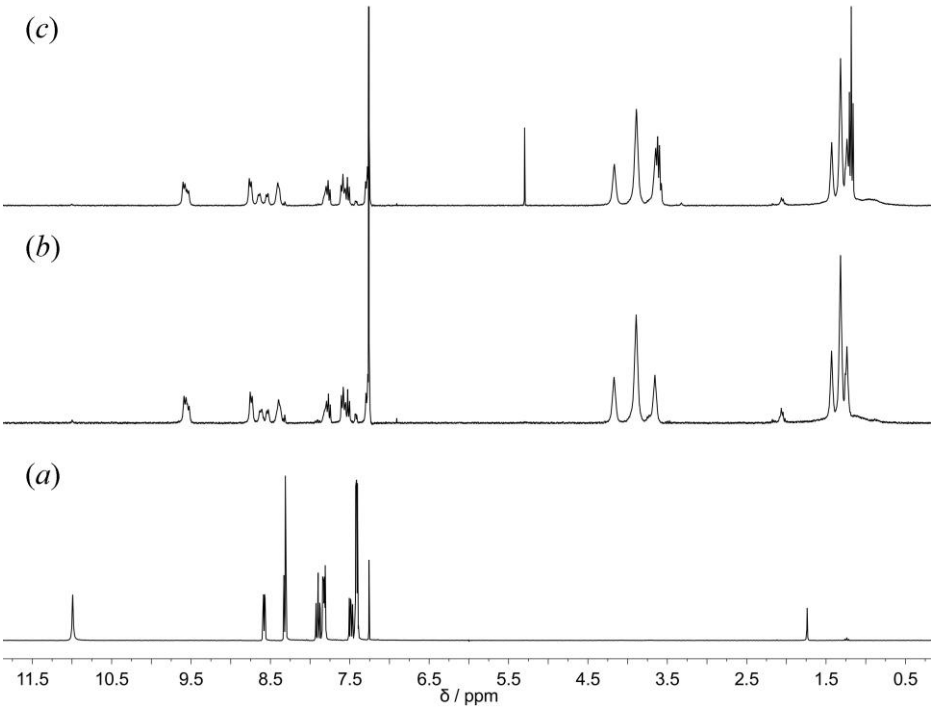

Fig. 1 ^{1}H NMR (300 MHz, Chloroform-*d*) spectra of (*a*) Hbphz, (*b*) [{Nd(pyrdtc)$_2$}$_2$(μ-bphz)$_2$] and (*c*) [{Nd(pyrdtc)$_2$(EtOH)}$_2$(μ-bphz)$_2$].

3.1 Synthesis and characterization of (*E*)-*N*-benzylidenepicolinohydrazide (Hbphz)

The hydrazone, Hbphz, was synthesized by a one-pot condensation reaction of equimolar amounts of 2-pyridinecarboxylic acid hydrazide and benzaldehyde in ethanol in 73% yield [20,21]. The product was characterized by elemental analysis, X-ray diffraction analysis, and IR and ^{1}H NMR spectroscopy. The ^{1}H NMR spectrum (Fig. 1*a*) suggested that the isolated hydrazone was a single product of possible *E* and *Z* isomers. The X-ray crystallographic analysis (Table S1) revealed the molecular structure of Hbphz as an *E*-isomer, which is depicted in Fig. 2*a*. The molecule has an almost planar structure; the planes of the pyridyl (N1, C1–C5) and phenyl (C8–C13) rings form a dihedral angle of 10.4(1)°. The plane defined by the central hydrazone linkage, –C=N–N–C(=O)–, is tilted by 8.0(1) and 16.4(1)°, respectively, to the planes of the pyridyl and phenyl rings. The hydrazone C6=O1 bond length, 1.226(3) Å, indicates a ketonic character [7], and the imine N3=C7 bond length, 1.279(3) Å, shows its double bond character, while the N2–N3 and N2–C6 bond lengths are 1.381(2) and 1.356(3) Å, respectively. Therefore, the N2 atom should have an amide-H atom. Intermolecular N–H···O hydrogen bonds form a one-dimensional chain structure (Fig. 2*b*), running along the *b*

axis. The UV-visible absorption spectra of Hbphz (Fig. S1) showed a characteristic intense band due to the π→π* transition centered at 306 nm.

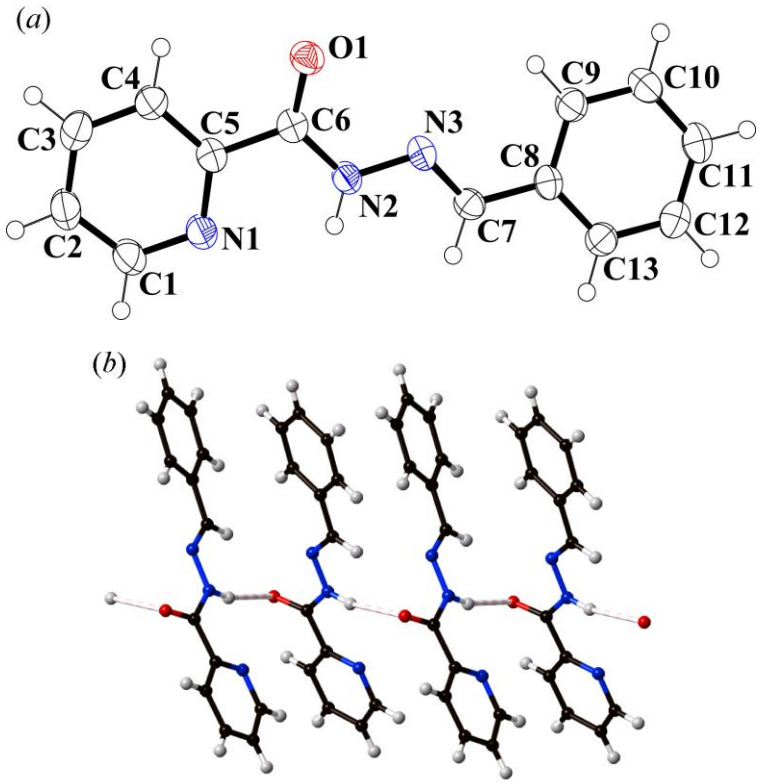

Fig. 2 (*a*) An ORTEP drawing of Hbphz (at 50% probability level), and (*b*) hydrogen-bonding interaction in the crystal of Hbphz.

3.2 Synthesis and characterization of Ln^{III} complexes with the hydrazonate, $bphz^{-}$

A reaction of Hbphz, $LnX_3 \bullet 6H_2O$ (Ln = La, Pr, Nd, Sm or Eu; X = Cl^- or NO_3^-), and sodium dimethyldithiocarbamate {$Na(Me_2dtc)$} or ammonium pyrrolidinedithiocarbamate {$NH_4(pyrdtc)$} in a 1:1:2 molar ratio in the presence of Et_3N in methanol at room temperature gave a pale-yellow or green precipitate of the respective $Ln^{III}(bphz)(RR'dtc)_2$ complexes {Ln = La (**1x**), Pr (**2x**), Nd (**3x**), Sm (**4x**) or Eu (**5x**); *RR′* = Me_2 (**x** = **a**) or pyr (**x** = **b**)} (Scheme 2). Recrystallization of each product from dichloromethane (or chloroform) and ethanol (or methanol) afforded single-crystals suitable for the X-ray diffraction study. The elemental analysis of these products suggested the composition of $Ln(bphz)(RR'dtc)_2 \bullet n$(solvent).

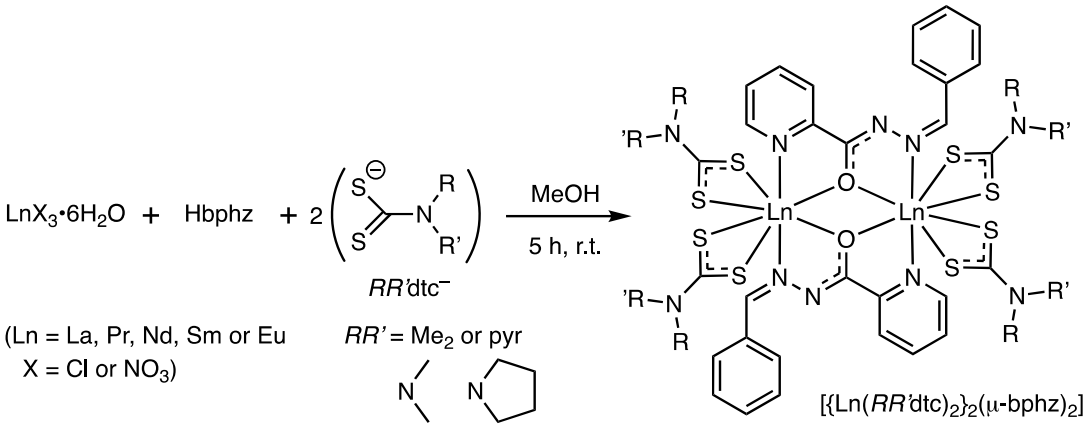

Scheme 2 Synthetic route of the bphz-bridged complexes

Figure S2 showed the FT-IR spectra of Hbphz and its complexes **3b** and **5b** as representative examples; other pyrdtc complexes of **1b**, **2b** and **4b** gave a similar spectral pattern. Also, the Me_2dtc complexes **1a–5a** showed similar IR spectra to one another. The ν(N–H) and ν(C=O) stretching bands appeared at 3212 cm^{-1} and 1664 cm^{-1}, respectively, in the spectrum of free Hbphz were disappeared in the spectra of the complexes, which indicated that the ligand has an anionic (i.e. $bphz^-$) and enolate character [22]. The $\nu(C{=}N)_{imine}$ and ν(N–N) bands observed at 1522 and 1141 cm^{-1}, respectively, in the free Hbphz were shifted to higher wavenumber regions on complexation, suggesting the coordination of the imine-N donor to a Ln^{III} ion [1]. The ν(C–S) and ν(C–N) bands associated with the $pyrdtc^-$ ligand in the complexes appeared at 1007 and 1430 cm^{-1} in **3b** and 1005 and 1436 cm^{-1} in **5b**, respectively.

3.3 Crystal structure of the complexes

Further characterization of the bphz complexes, **1a**–**5b**, were performed by the single-crystal X-ray analysis. The crystallographic data are summarized in Table S1 in the Supporting Information. The selected structural parameters are listed in Table 1.

The Eu^{III}–pyrdtc complex, **5b**, was crystallized in a monoclinic space group *Cc* (with *Z* = 4), and the asymmetric unit contains two Eu^{III} ions, each of which attaches two bidentate *S,S'*-donating $pyrdtc^-$ ligands, two bridging $bphz^-$ (deprotonated hydrazonate) anions and three chloroform molecules of crystallization: $[\{Eu(pyrdtc)_2\}_2(\mu\text{-}bphz)_2]\bullet 3CHCl_3$ (Fig. 3). The $bphz^-$ anions are bridged two Eu^{III} ions in a μ-1κ^2*N*(py),*O*:2κ^2*O*,*N*(imine) mode and form a

head-to-tail type $Eu_2(\mu\text{-bphz})_2$ core. Each Eu^{III} center accomplishes a distorted dodecahedral 8-coordination geometry with $N_2O_2S_4$ donor atoms, and two pyrdtc ligands in the mutually pseudo-*trans* positions are almost co-planar and perpendicular to the $Eu_2(bphz)_2$ plane (Fig. 3*b*). Analogous Eu^{III}–Me_2dtc complex, **5a**, was crystallized in a triclinic space group $P\bar{1}$ with $Z = 1$ (based on the dinuclear unit). The asymmetric unit consists of an Eu^{III} ion, two bidentate *S,S'*-donating Me_2dtc^- anions, and a bidentate *N*(py),*O*-bonding $bphz^-$ anion, but the symmetry expansion by the crystallographic inversion center forms further coordination of the neighboring $bphz^-$ anion via a bidentate *O*,*N*(imine) mode. Thus, the molecule has a C_i symmetric (head-to-tail type) bphz-bridged dinuclear structure, as similar to the above pyrdtc complex: $[\{Eu(Me_2dtc)_2\}(\mu\text{-bphz})_2]$ (Fig. S3).

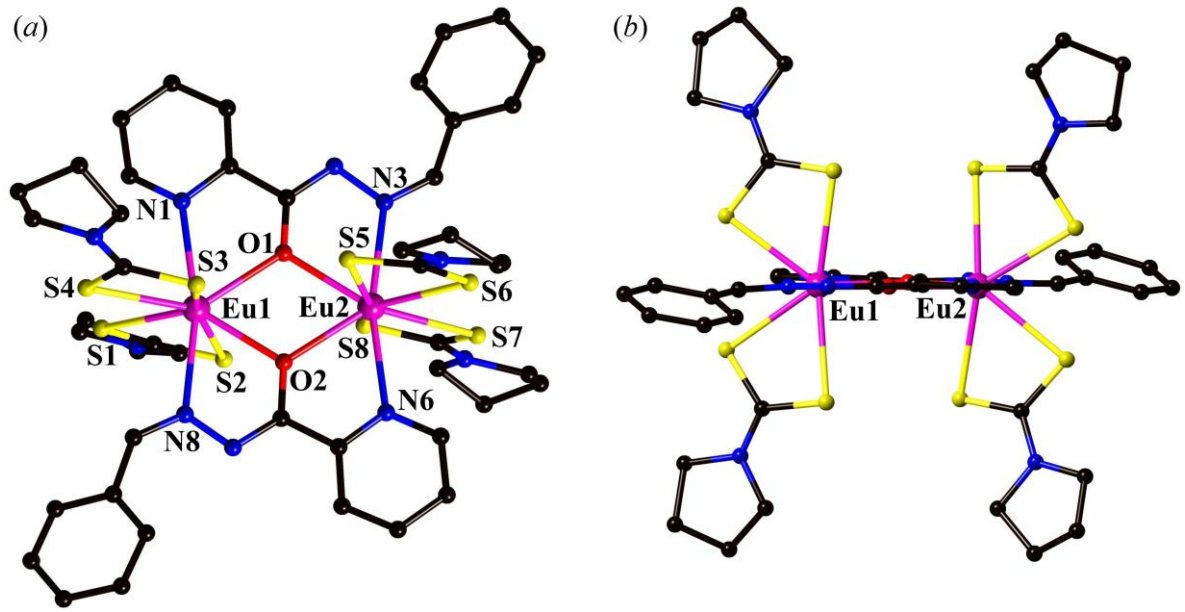

Fig. 3 (*a*) A perspective view of dinuclear complex of $[\{Eu(pyrdtc)_2\}_2(\mu\text{-bphz})_2]$ in **5b**•$3CHCl_3$ and (*b*) its side view from the $Eu_2(bphz)_2$ plane. Hydrogen atoms and lattice solvent molecules are omitted for clarity.

The Sm^{III}–Me_2dtc complex, **4a**, is isomorphorous to that of **5a**, and a similar molecular structure is resulted: $[\{Sm(Me_2dtc)_2\}(\mu\text{-bphz})_2]$ (Fig. S4). In the case of Sm^{III}–pyrdtc complex of **4b**, a similar dinuclear molecular structure with two solvent CH_2Cl_2 molecules of crystallization, $[\{Sm(pyrdtc)_2\}_2(\mu\text{-bphz})_2]$•$2CH_2Cl_2$ (Fig. S5) was obtained in a triclinic space group $P\bar{1}$ with $Z = 1$ (based on the dinuclear unit).

All four complexes of Eu^{III} and Sm^{III}, **4a**, **4b**, **5a** and **5b**, have similar structural features with two Ln^{III} ions having a $N_2O_2S_4$ dodecahedral 8-coordination and two bridging monodeprotonated hydrazonate anions ($bphz^-$). Compared to the metric parameters of the complexes with those of free Hbphz, the C=O and C–N bonds become longer (by ca. 0.07 Å) and shorter (by ca. 0.05 Å), respectively, while the N–N and N=C(imine) bond lengths are not different so much. This fact indicates that delocalization of the anionic character of the hydrazonate is limited in the [O=C–N] moiety, although the whole hydrazonato moiety [–C(=O)–N–N=C–] has a planar structure. Two Ln^{III} ions are placed on the hydrazonato planes, and the pyridine ring is also coplanar, while the phenyl ring of $bphz^-$ is slightly tilted from the planes (Table S2). Two *RR'*dtc ligands at each Ln^{III} ion are located above and below the $Ln_2(\mu\text{-bphz})_2$ plane, i.e., at mutually pseudo *trans*-positions, and their coordination planes are almost parallel to each other but perpendicular to the $Ln_2(\mu\text{-bphz})_2$ plane. The coordination bond lengths around Eu^{III} or Sm^{III} centers are: Ln–S, 2.85–2.93 Å; Ln–N, 2.50–2.62 Å; Ln–O, 2.75–2.41 Å, the bite angles of *RR'*dtc are 61.8–62.5°, and the bridging angles of Ln–O–Ln are 112.2–113.6°.

In contrast to the above complexes, the La^{III} complexes of **1a** and **1b** were found to have a different molecular structure (Fig. 4 and Fig. S6, respectively) in the crystals. The Me_2dtc complex of **1a** was crystallized in a monoclinic space group $P2_1/n$ with $Z = 2$ (based on the dinuclear unit), and the pyrdtc complex of **1b** was crystallized in a triclinic space group $P\bar{1}$ with $Z = 1$ (based on the dinuclear unit). Both complexes showed a dinuclear bphz-bridged $La^{III}_2(\mu\text{-bphz})_2$ structure having a crystallographic inversion center in the molecule. The bridging mode of the hydrazonato is the same as those in the Eu^{III} and Sm^{III} complexes, but the coordination bond lengths around the La^{III} are longer by 0.15–0.20 Å, which is consistent with the longer ionic radius of La^{III} than Eu^{III} and Sm^{III}. Because of the larger ionic size, the La^{III} center is deviated from the plane defined by two bridging ligands (Fig. 4*b*). In addition, the La^{III} center is coordinated by an ethanol molecule as well as two dithiocarbamato (*RR'*dtc^-) ligands. The coordinated ethanol molecule is hydrogen-bonded to one of the S atoms of *RR'*dtc^- ligand coordinated to the other La^{III} center (O2–H···S4: Fig. 4*a*). Two dithiocarbamato ligand

planes are almost perpendicular to each other and to the bridging bphz ligand plane, and, therefore, the coordination geometry around each La^{III} center is characterized as a 9-coordinate tricapped trigonal prism.

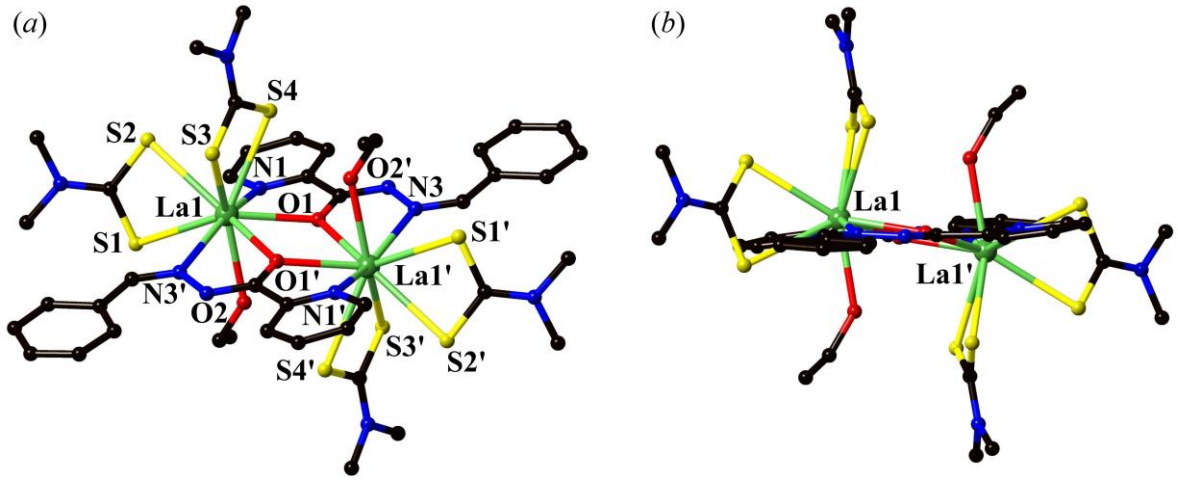

Fig. 4 (*a*) A perspective view of dinuclear complex of [{La(Me$_2$dtc)$_2$(EtOH)}$_2$(μ-bphz)$_2$] in **1a** and (*b*) its side view from the (μ-bphz)$_2$ plane. Hydrogen atoms and lattice solvent molecules are omitted for clarity.

Since the La^{III}(*RR'*dtc)$_2$ fragments form a 9-coordinate dinuclear bphz-bridged complex with a coordinated EtOH ligand, while the corresponding Sm^{III} and Eu^{III} ones gave an 8-coordinate dinuclear complexes where two dithiocarbamato ligand planes at each Ln^{III} center are co-planar, it is interesting to investigate the molecular structures of the Pr^{III} and Nd^{III} analogues. The Pr^{III}–pyrdtc complex of **2b** and the Nd^{III}–pyrdtc complex of **3b** were found to be isomorphous to the La^{III}–pyrdtc complex of **1b**, and a similar molecular structure with 9-coordinate Pr^{III} ions (Fig. S7) or Nd^{III} ions (Fig. S8) resulted in. The structural characteristics of **2b** and **3b** are also the same as those of **1b**. The coordination bond lengths around Pr^{III} center in **2b** are slightly shorter than the corresponding ones around La^{III} in **1b** by 0.02–0.06 Å and those around Nd^{III} in **3b** are further shorter by ca. 0.01 Å, although the Pr^{III} and Nd^{III} centers in **2b** and **3b** are still not on the plane of the bridging bphz ligands (Figs. S7*b* and S8*b*).

The crystal structure of Pr^{III}–Me$_2$dtc complex, **2a**, was found to be rather different from the above examples. It was crystallized in a triclinic space group $P\bar{1}$ with $Z = 4$ (based on the dinuclear unit), and its asymmetric unit contains a whole molecule of bphz-bridged dinuclear

Pr^{III} complex, two fragments of '$Pr^{III}(Me_2dtc)_2(bphz)$' which gives a dinuclear bphz-bridged complex by symmetry operation, and four molecules of solvent CH_2Cl_2 molecules; thus, the crystals of **2a** can be assigned as $[\{Pr(Me_2dtc)_2\}_2(\mu\text{-bphz})_2]\bullet 2CH_2Cl_2$. There are three kinds of crystallographically different dinuclear complexes, but all of them are found to be 8-coordinate around the Pr^{III} centers (Fig. S9). The characteristics of the molecular structures are also similar to those of the Sm^{III}_2 and Eu^{III}_2 complexes of **4a** and **5a**.

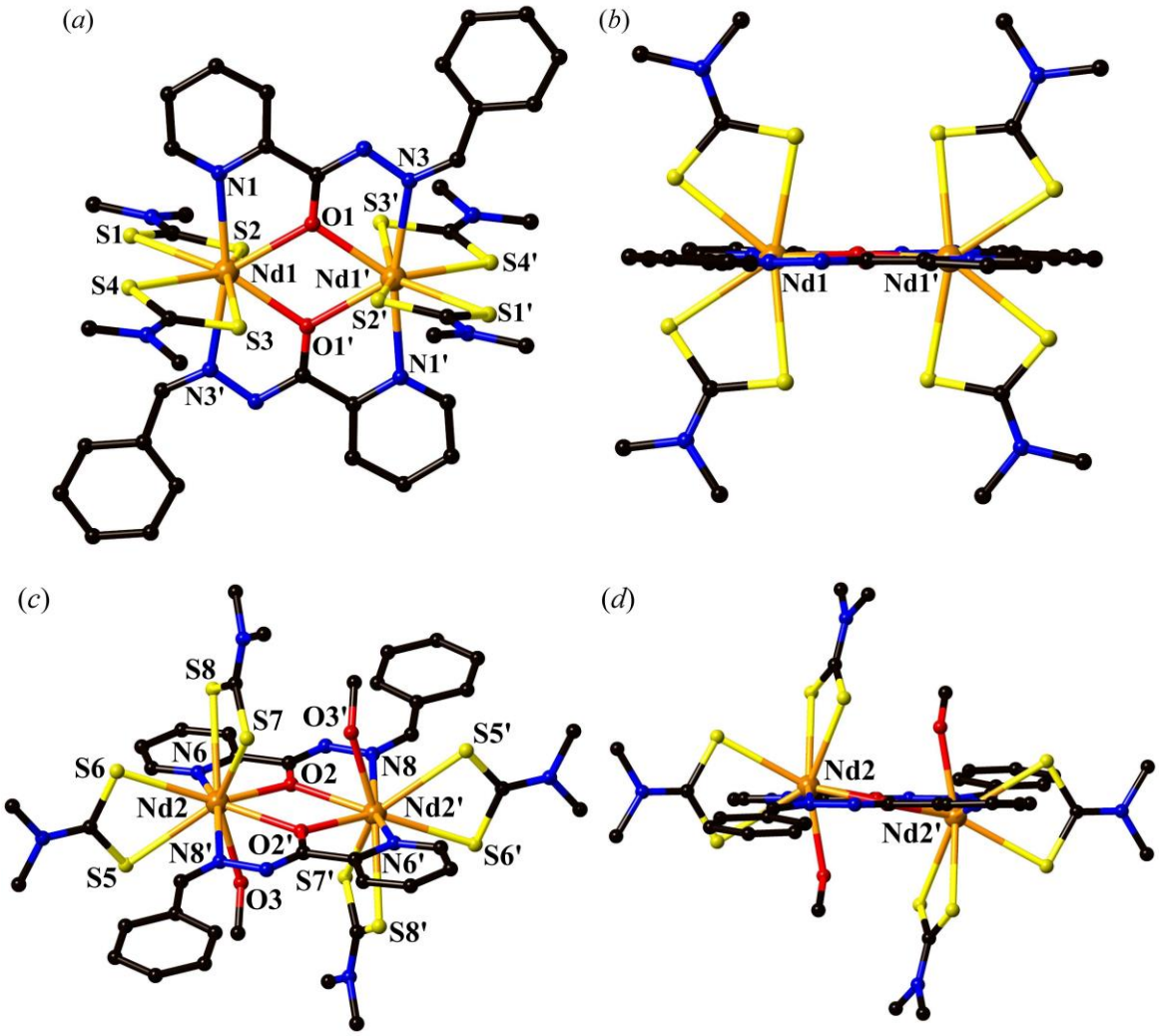

Fig. 5 Perspective views of (*a* and *b*) a 8:8-coordinate dinuclear complex of $[\{Nd(Me_2dtc)_2\}_2(\mu\text{-bphz})_2]$ and (*c* and *d*) a 9:9-coordinate dinuclear complex of $[\{Nd(Me_2dtc)_2(MeOH)\}_2(\mu\text{-bphz})_2]$ in **3a** (*b* and *d* are their side views from the $(\mu\text{-bphz})_2$ plane. Hydrogen atoms and lattice solvent molecules are omitted for clarity.

The Nd^{III}–Me_2dtc complex, **3a**, showed a further characteristic crystal structure (Fig. 5). It was crystalized in a triclinic space group $P\bar{1}$ with $Z = 2$ (based on the dinuclear unit), and the

asymmetric unit contains two halves of the dinuclear bphz-bridged Nd^{III} molecules and two solvent $CHCl_3$ molecules. Interestingly, these two fragments have different molecular structures; one of the molecules (with Nd1) has a similar 8-coordinate structure (Fig. 5*a* and *b*) to those of the Sm^{III} (**4a**) and Eu^{III} (**5a**) analogues (where two mutually *trans*-positioned Me_2dtc ligand planes are co-planar to each other), while the other molecule (with Nd2) is coordinated by an additional MeOH molecule to complete a 9-coordinate coordination geometry (Fig. 5*c* and *d*). Therefore, the crystals is assigned as $[\{Nd(Me_2dtc)_2\}_2(\mu\text{-bphz})_2]\bullet[\{Nd(Me_2dtc)_2(MeOH)\}_2(\mu\text{-bphz})_2]\bullet 4CHCl_3$.

The above-mentioned crystallographic analyses suggested that the bphz-bridged dinuclear lanthanoid dithiocarbamato complexes tend to form a 9-coordinate complex by a coordination of solvent EtOH (or MeOH) molecule used for recrystallization, when a larger Ln^{III} ion (e.g., La^{III}, Pr^{III} or Nd^{III}) was applied. Then, an interesting question arose; would an 8:8- or 9:9-coordinate molecule be obtained by recrystallizing these complexes from non-coordinating solvents? We have attempted several crystallization and finally isolated pale green and block single-crystals of the Nd^{III}–pyrdtc complex, **3b'**, from a mixture of dichloromethane and diethyl ether. Although the crystallinity was not good enough to obtain a satisfactory *R* value, we have confirmed the successful crystallization of the 8:8-coordinate $[\{Nd(pyrdtc)_2\}_2(\mu\text{-bphz})_2]$ (**3b'**) complex (Table S1 and Fig. S10).

3.4 Spectroscopic Properties

3.4.1 ^{1}H NMR study

The ^{1}H NMR spectra of Hbphz and some Ln^{III} complexes in chloroform-*d* were measured. As representative examples, the spectra of free Hbphz and the Nd^{III}–pyrdtc complexes with 9:9- and 8:8-coordinate structures, $[\{Nd(pyrdtc)_2(EtOH)\}_2(\mu\text{-bphz})_2]$ (**3b**) and $[\{Nd(pyrdtc)_2\}_2(\mu\text{-bphz})_2]$ (**3b'**), which were obtained by recrystallization from dichloromethane/ethanol and dichloromethane/diethyl ether, respectively, are shown in Fig. 1. In the spectrum of free Hbphz (bottom), the amide (NH) and imine (N=CH) proton resonances are observed at δ 10.99 and 8.58, respectively. In addition, multiplet resonances due to the aromatic (CH) protons are observed in the range of δ 7.31–8.42. The Nd^{III}_2 complexes gave

relatively sharp resonances in the typical range (δ 10–0) for diamagnetic compounds (middle and top), although they contain Nd^{III} ions. In these spectra, the disappearance of the amide NH resonance indicates the deprotonation from the hydrazone. The resonance for the imine (N=CH) proton is observed at δ 9.56, while those for the aromatic (CH) protons occurred in the range of δ 7.26–8.94. The methylene (CH_2) protons of $pyrdtc^-$ ligands gave two pseudo triplets around δ 3.8 and 1.3. In addition, in the spectrum of **3b** three sharp resonances due to free ethanol are observed [23]. These spectral features of **3b** and **3b'** suggest that the EtOH (or MeOH) molecule in the 9:9-coordinate complex dissociates in a chloroform solution to exist as an 8:8-coordinate dinuclear bphz-bridged complex.

3.4.2 UV-visible absorption and MCD spectra

UV-visible absorption and MCD spectra of the $pyrdtc^-$ complexes, **1b**–**5b**, were measured in CH_2Cl_2 solutions. The complexes exhibited similar absorption spectral pattern in the UV region-as shown in Fig. S11. The band at 340 nm was assigned to the intra-ligand charge transfer transition [24,25]. In the visible region, sharp but weak absorption bands and MCD signals characteristic of f–f transitions were observed in the complexes. The spectra are presented in Figs. 6–9 and discussed below.

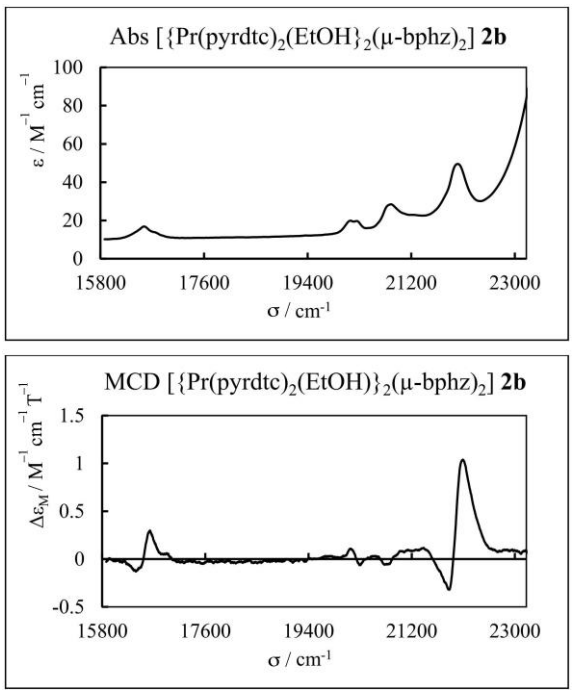

Fig. 6. Absorption (top) and MCD (bottom) spectra of [{Pr(pyrdtc)$_2$(EtOH)}$_2$(μ-bphz)$_2$] **2b**.

The absorption spectrum of **2b** (Fig. 6, top) shows four sharp but weak bands at 16580, 20200, 20830 and 22050 cm^{-1}. These bands are due to the f–f transition from the ground state $^3H_4$ to the $^1D_2$, $^3P_0$, ($^3P_1$,$^1I_6$) and $^3P_2$ excited states, respectively, which are based on the reported signal assignments for an aqueous $Pr(NO_3)_3$ and $Pr(ClO_4)_3$ solutions [26]. In the MCD spectrum (bottom), the f–f transition bands are observed as characteristic positive *A*-term MCD signals at 16500 and 21930 cm^{-1}, while negative *A*- and *C*-term MCD signals at 20240 and 20830 cm^{-1}, respectively.

The absorption spectrum (top) of complex **3b** (Fig. 7) shows four sharp but weak f–f bands with maximum peaks at 12420, 13320, 17040 and 18800 cm^{-1}, which are assigned to the $^4I_{9/2} \rightarrow (^4F_{5/2}, ^4H_{9/2})$, $(^4S_{3/2}, ^4F_{7/2})$, $(^2G_{7/2}, ^4G_{5/2})$ and $^4G_{7/2}$ transitions, respectively. The $^4I_{9/2} \rightarrow (^4F_{5/2}, ^4H_{9/2})$, $(^4S_{3/2}, ^4F_{7/2})$ and $(^2G_{7/2}, ^4G_{5/2})$ transitions occurred at slightly lower in energies than those of a similar hydrazone-based Nd^{III} complex reported by Singh et al [27]. Compared to the related Nd^{III} complex with *N*-(furfuralidene)-*N*-isonicotinoylhydrazine [28], only the $^4I_{9/2} \rightarrow (^4F_{5/2}, ^4H_{9/2})$ band was consistent, and the other transitions occurred at lower energies. In the MCD spectrum (bottom), the MCD signals were observed at 12380, 13290, 13500, 16910 and

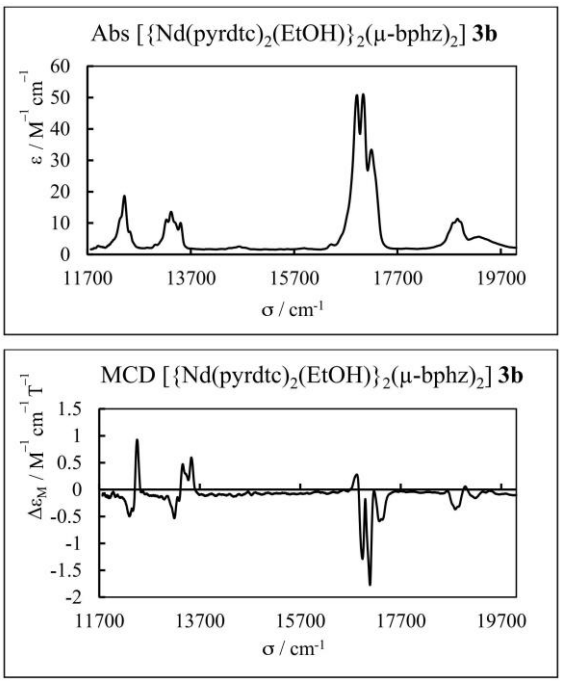

Fig. 7. Absorption (top) and MCD (bottom) spectra of [{Nd(pyrdtc)$_2$(EtOH)}$_2$(μ-bphz)$_2$] **3b**.

17040 cm^{-1}. These signals are dominated by room temperature *C*-terms, except for the signal at 12380 cm^{-1} which appeared as a positive pseudo *A*-term [29].

The characteristic $^4I_{9/2} \rightarrow (^4G_{5/2},^2G_{7/2})$ hypersensitive transition exhibits splitting at 16910 and 17040 cm^{-1}. These crystal-field splitting was also observed in the second derivative absorption spectra of $Nd(C_2H_3O_2)_3H_2O$ **[**30] and neodymium complex with fleroxacin [31] at higher energies. The $^4I_{9/2} \rightarrow (^4G_{5/2}, ^2G_{7/2})$ hypersensitive transition *C*-term MCD signals are more clearly resolved in **3b** than those in previously reported mononuclear Nd^{III} analogues [29].

In Fig. 8 (top), no f–f bands were detected in the absorption spectrum for complex **4b** probably because they were overlapped or buried underneath the strong metal-ligand charge–transfer band around 24000 cm^{-1} [28, 32]. In the MCD spectrum (bottom), the structure of the MCD bands is very complicated due to the Zeeman splitting of the ground state and all the excited states [33]. Two characteristic MCD signals showing a positive *A*-term and a negative *C*-term occurred at 23510 and 21260 cm^{-1}, owing probably to the f–f transition from the $^6H_{6/2}$ ground state to the $^6P_{3/2}$ and $^4I_{13/2}$ excited states, respectively.

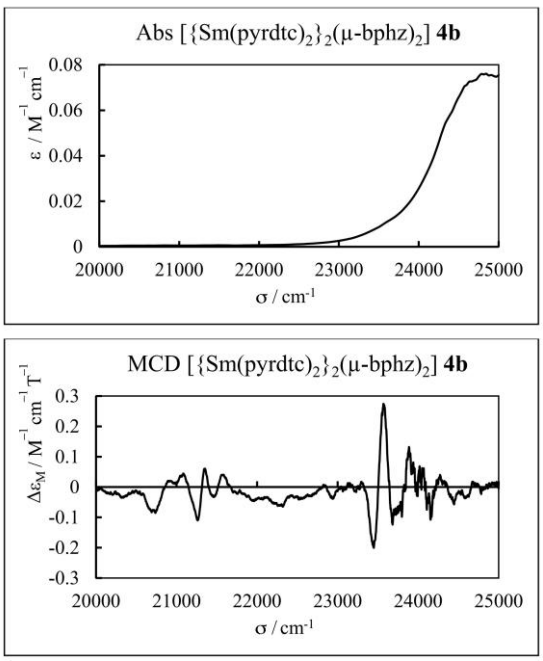

Fig. 8. Absorption (top) and MCD (bottom) spectra of [{Sm(pyrdtc)$_2$}$_2$(μ-bphz)$_2$] **4b**.

In Fig. 9 (top), complex **5b** exhibited two very weak bands at 21450 and 21460 cm^{-1} which would be assigned to the $^7F_0 \rightarrow {}^5D_2$ transition. The positions of these bands are in good

agreement, but the shapes are different from previously reported spectra of mononuclear [Eu(*RR'*dtc)$_3$(NN)] (*RR'* = dimethyl-, pyrrolidine- and *S*-prolinol-; NN = 1,10-phenanthroline or 2,2'-bipyridine) complexes [29]. In the MCD spectrum (bottom), a negative pseudo *A*-term MCD signal is observed at 21430 cm^{-1} and corresponds to the absorption bands. The shape of the negative pseudo *A*-term of **5b** is different from that of the negative *B*-term observed in the previously reported mononuclear Eu^{III} dithiocarbamato complexes [29]. The MCD results show that the coordination environment of the lanthanoid with a mixed N,O,S donor set gives a significant difference in the electronic structure from that of an N,S donor set. This finding shows that the sensitivity of the MCD technique [34] can be used as an effective tool to probe the electronic structure(s) and physical properties of Ln^{III} complexes in solution.

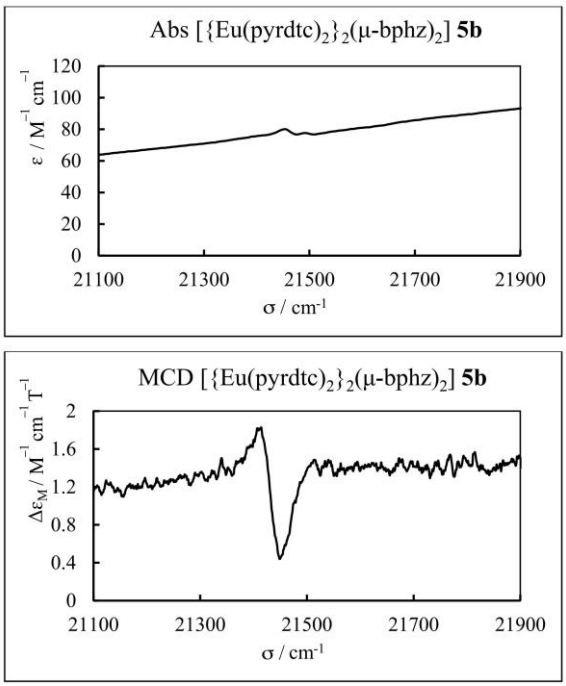

Fig. 9. Absorption (top) and MCD (bottom) spectra of [{Eu(pyrdtc)$_2$}$_2$(μ-bphz)$_2$] **5b**.

4. Conclusion

A series of novel hydrazonato-bridged homodinuclear Ln$^{III}_2$ dithiocarbamato complexes were prepared and their crystal and molecular structures and spectroscopic properties were investigated. The crystal structures revealed that the early Ln^{III} ions tend to crystallize as a 9:9-coordinate complex with the ninth position occupied by a solvent alcohol molecule, while the

middle Ln^{III} ions deposit the crystals of only 8:8-coordinate complex. The coordination of a deprotonated monoanionic hydrazonato ligand was confirmed by the IR and ^{1}H NMR spectroscopy. Similar spectral patterns of ligand-centered and Laporte forbidden f–f transitions were observed in the UV-visible spectral region. The MCD parameters exhibited by the complexes demonstrate their potential in magneto-optical applications. In addition, these hydrazonato-bridged dinuclear lanthanoid(III) complexes with some suitable modification would be used as an effective building block for supramolecular chemistry. In particular, the late (heavier) Ln^{III} ions would be interesting in their magnetic and catalytic properties. Such an investigation of a series of complexes are now in progress in our laboratory.

Competing interest

The authors declare no conflict of interest in relation to this work.

Acknowledgements

The authors wish to thank Dr. Yukinari Sunatsuki of his assistance in the crystallographic analysis. This work was supported by a Grant-in-Aid for Scientific Research No. 18K05146 from the Ministry of Education, Culture, Sports, Science, and Technology, Japan.

Appendix A. Supplementary data

Details of the crystal structures and the infrared and UV-visible absorption spectra of the complexes in PDF format. Crystallographic data for compounds Hbphz and complexes **1a–5b** have been deposited with the Cambridge Crystallographic Data Centre, CCDC 1944410–1944421. These data can be obtained free of charge from The Cambridge Crystallographic Data Centre via www.ccdc.cam.ac.uk/data_request/cif.

References

1. R.S. Baligar, V.K. Revankar, *J. Serb. Chem. Soc.,* 71 (2006) 1301.
2. B. Moksharagni, K.H. Reddy. *Eur. J. Biom. Pharm. Sci.*, 5 (2018) 810.

3. B. Parmar, K.K. Bisht, P. Maiti, P. Paul, E. Suresh, *J. Chem. Sci.*, 126 (2014) 1373.
4. M. Chang, H. Horiki, K. Nakajima, A. Kobayashi, H.-C. Chang, M. Kato, *Bull. Chem. Soc. Jpn.*, 83 (2010) 905.
5. A. Mori, T. Suzuki, Y. Sunatsuki, M. Kojima, *Bull. Chem. Soc. Jpn.*, 88 (2015) 480.
6. S. Biswas, S. Das, G. Rogez, V. Chandrasekhar, *Eur. J. Inorg. Chem.*, (2016) 3322.
7. M.U. Anwar, S.S. Tandon, L.N. Dawe, F. Habib, M. Murugesu, L.K. Thompson, *Inorg. Chem.*, 51 (2012) 1028.
8. N.C. Anastasiadis, I. Mylonas-Margaritis, V. Psycharis, C.P. Raptopoulou, D.A. Kalofolias, C.J. Milios, N. Klouras, S.P. Perlepes, *Inorg. Chem. Comm.*, 51 (2015) 99.
9. L. Zhang, Q.-Y. Zhang, P. Zhang, L. Zhao, M. Guo, J. Tang, *Inorg. Chem.*, 56 (2017) 7882.
10. A. Gusev, R. Herchel, I. Nemec, V. Shul'gin, I.L. Eremenko, K.Lyssenko, W.Linert, Z. Trávníček, *Inorg. Chem.*, 55 (2016) 12470.
11. W.M. Faustino, O.L. Malta, E.E.S. Teotonio, H.F. Brito, A.M. Simas, G.F. de Sá, *J. Phys. Chem.,* A110 (2006) 2510.
12. P. Pitchaimani, K.M. Lo, K.P. Elango, *Polyhedron*, 93 (2015) 8.
13. A. Yakubu, T. Suzuki, M. Kita. *J. Chem. Educ.*, 94 (2017) 1357.
14. (a) Rigaku Co. Ltd., Process−Auto, Akishima, Tokyo, 1998. (b) Rigaku Co., Ltd., CrystalClear, Akishima, Tokyo, 1998–2015.
15. Rigaku Co. Ltd., NUMABS, Akishima, Tokyo, 1999.
16. M.C. Burla, R. Caliandro, M. Camalli, B. Carrozzini, L.G. Cascarano, L. De Caro, C. Giacovazzo, G. Polidori, D. Siliqi, R. Spagna, SIR2008. *J. Appl. Cryst.*, 40 (2007) 609.
17. M.G. Sheldrick, SHELXT Version 2014/5. *Acta Cryst.*, A70 (2014) C1437.
18. M.G. Sheldrick, SHELXL Version 2014/7. *Acta Cryst.*, A64 (2008) 112.
19. Rigaku Co. Ltd., CrystalStructure 4.3, Akishima, Tokyo, 2000−2018.
20. A. Mori, T. Suzuki, Y. Sunatsuki, A. Kobayashi, M. Kato, M. Kojima, K. Nakajima, *Eur. J. Inorg. Chem.*, (2014) 186.
21. J. Qin, Q. Yin, S.-S. Zhao, J.-Z. Wang, S.-S. Qian, *Acta Chim. Slov.*, 63 (2016) 55.

22. V.C. Havanur, D.S. Badiger, S.G. Ligade, K.B. Gudasi, *Der Pharma Chemica*, 3 (2011) 292.
23. P. Pitchaimani, M.L. Lo, K.P. Elango, *J. Coord. Chem.*, 68 (2015) 2167.
24. M. Mahato, P.P. Jana, K. Harms, H.P. Nayek, *RSC Adv.*, 5 (2015) 62167.
25. V. Vrdoljak, G. Pavlovic, T. Hrenar, M. Rubci, P. Siega, R. Dreos, M. Cindri, *RSC Adv.,* 5 (2015) 104870.
26. C. Görller-Walrand, L. Fluyt, Magnetic circular dicroism of lanthanides, Handb. Phys. Chem. Rare Earths, 40 (2010) 1–107.
27. B. Singh, T.B. Singh, *Indian J. Chem.*, 38A (1999) 1286.
28. S.S. Devi, A.M. Singh, *J. Chem. Pharm. Res.*, 3 (2011) 399.
29. A. Yakubu, T. Suzuki, M. Kita, *Inorg. Chim. Acta*, 484 (2019) 394.
30. S.V.J. Lakshman, S. Buddhudu, *Proc. Indian natn. Sci. Acad.*, 47 A(6) (1981) 721.
31. N. Wang, W. Jiang, X. Xu, Z. Si, H. Bai, C. Tian, *Anal. Sci.*, 18 (2002) 591.
32. C. Su, M. Tan, N. Tang, X. Gan, W. Liu, X. Wang, *J. Coord. Chem., 38* (1996) 207
33. C. E. Secu, S. Polosan, M. Secu, *Journal of Luminescence,* 131 (2011) 1747.
34. K. Binnemans, *Coord. Chem. Rev.*, 295 (2015) 1.

Table 1. Selected parameters of Ln^{III}_2 complexes.[a]

parameters	**1a**	**1b**	**2a**	**2b**	**3a**(mol1)[b]	**3a**(mol2)[b,c]	**3b**	**3b'**	**4a**	**4b**	**5a**	**5b**
Bond Lengths (Å)												
Ln1─S1	3.002(3)	3.015(3)	2.906(4)	2.968(2)	2.920(3)	2.973(2)	2.990(2)	2.899(2)	2.856(5)	2.876(1)	2.853(3)	2.867(3)
Ln1─S2	3.031(3)	3.000(3)	2.921(3)	2.982(2)	2.895(3)	2.941(3)	2.992(2)	2.940(1)	2.863(6)	2.884(1)	2.844(3)	2.877(5)
Ln1─S3	3.032(3)	3.029(3)	2.919(3)	3.006(2)	2.898(3)	2.970(2)	2.963(2)	2.903(2)	2.893(6)	2.932(1)	2.857(3)	2.921(5)
Ln1─S4	3.052(3)	3.032(3)	2.889(4)	2.999(3)	2.889(2)	2.986(3)	2.952(2)	2.890(2)	2.870(5)	2.865(1)	2.870(3)	2.854(4)
Ln1─N1	2.695(8)	2.688(10)	2.658(9)	2.627(8)	2.629(7)	2.637(7)	2.620(7)	2.627(5)	2.620(13)	2.586(4)	2.589(7)	2.577(11)
Ln1─N3*	2.692(7)	2.702(10)	2.585(9)	2.639(7)	2.573(6)	2.624(7)	2.632(6)	2.589(6)	2.530(12)	2.560(4)	2.510(7)	2.498(10)
Ln1─O1	2.506(5)	2.520(6)	2.451(8)	2.480(4)	2.430(5)	2.456(5)	2.464(4)	2.409(5)	2.405(10)	2.375(3)	2.380(5)	2.390(7)
Ln1─O1*	2.518(6)	2.543(8)	2.488(10)	2.499(6)	2.432(5)	2.484(5)	2.483(5)	2.444(4)	2.410(8)	2.412(3)	2.398(6)	2.392(9)
Ln1─$O2_{EtOH}$	2.583(7)	2.586(7)	–	2.549(6)	–	2.525(9)[d]	2.533(5)	–	–	–	–	–
C6─O1	1.297(9)	1.310(14)	1.294(13)	1.311(10)	1.312(9)	1.307(9)	1.286(9)	1.309(7)	1.301(17)	1.303(5)	1.297(10)	1.332(15)
C6─N2	1.332(10)	1.355(13)	1.329(17)	1.332(9)	1.329(10)	1.281(10)	1.329(8)	1.295(9)	1.327(16)	1.298(6)	1.302(9)	1.300(14)
Bond angles (°)												
S1─Ln1─S2	58.43(9)	58.57(8)	61.32(12)	59.30(6)	61.30(7)	59.44(9)	59.27(7)	61.58(5)	62.04(15)	62.12(3)	62.48(9)	62.35(11)
S3─Ln1─S4	57.63(8)	58.30(9)	61.38(11)	58.94(7)	61.56(8)	59.69(6)	59.74(6)	62.11(5)	61.79(14)	61.90(4)	62.15(8)	62.02(10)
Ln1─O1─Ln1*	115.48(19)	114.7(3)	111.9(3)	115.7(2)	113.3(2)	116.11(19)	115.5(2)	113.1(2)	112.2(4)	113.6(1)	112.9(2)	113.5(3)
Average												
Bond length (Å)												
Ln─S	3.029(4)	3.019(4)	2.909(7)	2.989(5)	2.900(4)	2.967(4)	2.974(4)	2.908(3)	2.871(1)	2.889(3)	2.856(6)	2.8798(9)
Ln─N	2.694(11)	2.695(14)	2.622(13)	2.633(11)	2.601(10)	2.631(11)	2.626(9)	2.608(8)	2.575(18)	2.573(6)	2.510(10)	2.538(15)
Ln─O	2.512(8)	2.532(10)	2.470(13)	2.490(7)	2.431(7)	2.470(7)	2.474(6)	2.427(6)	2.408(13)	2.394(4)	2.389(8)	2.391(21)
Bond angles (°)												
S─Ln1─S	58.03(12)	58.44(12)	61.35(16)	59.12(9)	61.43(10)	59.57(11)	59.51(9)	61.85(7)	61.9(2)	62.01(5)	62.3(12)	62.17(15)

[a]The asterisk (*) indicates the symmetry-related atom. [b]Mol1 and mol2 have 8:8- and 9:9-coordinate structures, respectively. [c]Atom-numberings of mol2 should be modified appropriately: see Supplementary Information for details. [d]Ln2–$O3_{MeOH}$.